ELSEVIER

Biochimica et Biophysica Acta 1463 (2000) 65–80

BIOCHIMICA ET BIOPHYSICA ACTA
BBA

www.elsevier.com/locate/bba

Ideally amphipathic β-sheeted peptides at interfaces: structure, orientation, affinities for lipids and hemolytic activity of $(KL)_mK$ peptides

Sabine Castano [a], Bernard Desbat [b], Jean Dufourcq [a,*]

[a] *Centre de Recherche Paul Pascal, Avenue A. Schweitzer, CNRS, 33600 Pessac, France*
[b] *Laboratoire de Physico-Chimie Moléculaire, Université de Bordeaux I, 33400 Talence, France*

Received 18 May 1999; received in revised form 7 September 1999; accepted 15 September 1999

Abstract

Designed to model ideally amphipathic β-sheets, the minimalist linear $(KL)_mK$ peptides ($m = 4$–7) were synthesized and proved to form stable films at the air/water interface, they insert into compressed dimyristoylphosphatidylcholine monolayers and interact with egg phosphatidylcholine vesicles. Whatever the interface or the lateral pressure applied to the films, FT-IR and polarization-modulated IRRAS spectroscopy developed in situ on the films indicated that all the peptides totally fold into intermolecular antiparallel β-sheets. Calculated spectra of the amide region allowed us to define the orientation of the β-strands compared to the interface. It is concluded that such β-sheets remain flat-oriented without deep perturbation of zwitterionic phospholipids. Dansyl labelling at the N-terminus indicates that all the peptides are monomeric at a low concentration in aqueous buffer and bind to lipids with similar Dns burying. The affinities for zwitterionic lecithin mono- and bilayers, quantitatively estimated from buffer to lipid partition constants, monotonically increased with peptide length, indicating that hydrophobicity is a limiting parameter for lipid and membrane affinities. Peptides induced permeability increases on zwitterionic liposomes, they are strongly hemolytic towards human erythrocytes and their activity increases concurrently with length. Taking into account the lipid affinity, a hemolytic efficiency can be defined: at the same amount of peptide bound, this efficiency strongly increases with the peptide length. It is proposed that the first determinant step of membrane disturbance is the invasion of the outer membrane leaflet by these ideally amphipathic β-sheeted structures lying flat at the interface, like large rafts depending on the number of β-strands.

Keywords: β-Sheeted peptide; Lipid–peptide interaction; Cytotoxic; FT-IR spectroscopy; Polarization-modulated IRRAS; Monolayer; Phospholipid vesicle; Fluorescence

1. Introduction

Short cytotoxic peptides isolated from the defense systems of diverse species commonly play both offensive and defensive roles against external aggressions. Some are specifically antimicrobial while others are cytotoxic against all types of cells, most act by enhancing the permeability of the biological membrane by a direct disturbance of the lipid matrix [1–4]. These peptides generally display a positive net charge and a high amphipathic character, most of them adopting amphipathic secondary structures, often

* Corresponding author. Fax: +33 (5) 56 84 56 00; E-mail: dufourcq@crpp.u-bordeaux.fr

0005-2736/00/$ – see front matter
PII: S0005-2736(99)00175-3

α-helical, in a lipid environment [1–3,5]. The enhancement of these parameters increases their binding ability and hence their membrane activity [6–10].

If amphipathic α-helical peptides gave rise to a huge literature [11], amphipathic β-sheeted ones have been less intensively studied [2]. They mainly display antimicrobial activities. Unlike many α-helical amphipathic peptides, only a few natural β-sheeted compounds are hemolytic [12,13], like cardiotoxins from snake venoms ($\approx$60 residues) [14,15] and the 10 residues cyclic gramicidin S [12].

Their β-sheeted structure is generally stabilized intramolecularly either by cyclization or by disulfide bridges. For instance, defensins from vertebrates [13,16–18], plants [18] or insects [3,19,20] are small proteins ($<$60 residues) containing a high amount of β-sheets stabilized by S–S bridges. That is also the case for the short tachiplesins and protegrins (16–18 residues) isolated from blood cells of horseshoe and pig crabs [18,21–23], the cationic dodecapeptide bactenecin from bovine neutrophils [24] and the 25 residue long bovine amphipathic lactoferricin B [25].

Only a few biophysical studies have been performed to define the mechanism of action of these natural β-sheeted peptides [13,14,21,23,26–28]. Some attempts were done to synthesize rationalized amphipathic [29–32] or totally apolar [33] β-structures but few studies were devoted to structure–function relationships in order to settle the peculiarities of the β-sheet motif when involved in toxins which induce a membrane permeability increase. A β-sheeted structure was established in the presence of lipids for some amphipathic oligopeptides such as $(VEOrn)_3V$ [31,34], $(LS)_n$ and $(VT)_n$ [31,35]. Model $(SVKV)_n$, $n=1$–3, and $(KV)_n$, $n=2$–4, peptides adopt β-structures in acidic phospholipid bilayers and also induce leakage from vesicles, but they are not antimicrobial [31]. A linear analog of cyclic tachiplesin I is less potent both in antibacterial activity and in lipid bilayer permeabilizing ability [21,23]. Synthetic analogs of gramicidin S, with various ring sizes, permeabilize acidic liposomes and are antimicrobial [12] while other cyclic gramicidin S analogs from 10 to 14 residues exhibit a β-sheet structure and are highly hemolytic [28].

Conformational studies in aqueous solution at the air/water interface and in C_{18}-membrane mimetic environment have been reported for only two LK peptides, namely $Fmoc(LK)_3L$ and $(KL)_9$ peptides [36,37]. Very recently, we showed that short linear L_iK_j ($i=2j$) peptides ($\leq$ nine residues) are β-sheeted and hemolytic without being ideally amphipathic [6,7,38].

In the present paper, we report a homologous series of synthetic linear $(KL)_mK$ peptides from 9 to 15 residues. These short basic peptides have a strict 2-fold periodicity in the sequence to generate ideally amphipathic β-strands, with a perfect segregation of the charged K residues on the same side of the putative intermolecular β-sheets. After an evaluation of their hemolytic activity, the evolution of their physico-chemical properties was systematically investigated using dansyl labelling. The conformation and orientation of peptides in situ at the interfaces, either air/water or inserted into a lipid monolayer on Langmuir troughs, were determined using the polarization-modulated IRRAS (PMIRRAS) technique [38–42]. The affinities for lipid mono- and bilayers were estimated to quantitatively correlate physical properties and biological activity of the peptides.

2. Materials and methods

2.1. Materials

Peptides were synthesized on solid phase using the base labile Fmoc-protecting group [43] by Fournier Pharma (Heidelberg, Germany) and purified by high performance liquid chromatography (HPLC) on a CN column eluted with a CH_3CN gradient. All were of $\geq$97% purity and their masses corresponded to the calculated ones. They were stored as dry powders at −20°C and dissolved in MeOH before use to give stock solutions of about 0.3 mM. All the peptides were amidated at the C-terminus and labelled at the N-terminus by a fluorescent dansyl group. Peptide concentrations were then estimated from absorbance measurements on a Pye Unicam Philips 8800 spectrophotometer with $\varepsilon^{Dns}_{340nm} = 4640\ M^{-1}\ cm^{-1}$ [44].

Egg phosphatidylcholine (EPC), prepared and purified from egg yolks as usually [6], was used as mixtures of EPC-cholesterol (EPC-Chol) (5%). Dimyristoylphosphatidylcholine (DMPC) from Avanti Polar Lipids (Birmingham, AL, USA) was solubilized in chloroform at about 5 mM.

The organic solvents, MeOH and $CHCl_3$ from Prolabo, Tris and calcein from Sigma and $CoCl_2$ and Triton X-100 from Aldrich-Chemie were the purest available.

2.2. HPLC analysis

The retention times (RT) of the peptides were measured by reversed phase (RP)-HPLC on a C_{18} reverse phase Purospher RP-18 end-capped semi-preparative column (125×4 nm, 5 μm particle size), in conjunction with a Waters millennium HPLC system as previously described [6].

2.3. Hemolytic assay

Fresh human blood from a healthy O^+ donor was collected on citrate and centrifugated at $980 \times g$ for 3 min. The erythrocyte pellet was washed three times in saline buffer (20 mM Tris, 130 mM NaCl, pH 7.4) and resuspended in buffer to obtain 10^7 cells/ml, which corresponded to an absorbance OD = 2.0 of Hb ($\varepsilon_{414} = 4.2 \times 10^5$ M^{-1} cm^{-1}). Experiments were performed as already described [6].

2.4. Lipid vesicle preparations

Small unilamellar vesicles (SUVs) were prepared from a lyophilized lipid mixture (EPC-Chol 20/1 molar ratio) hydrated by buffer (Tris 20 mM, pH = 7.4) at about 5–10 mM. After vortexing at 25°C, the dispersions were tip-sonicated under N_2 at a constant temperature (~10°C) for 10 min using a Vibracell 72405 apparatus. This gave SUVs as already checked by light scattering and gel filtration [45].

Large unilamellar vesicles (LUVs) composed of phosphatidylcholine and cholesterol, PC-Chol 20/1 molar ratio, were formed by extrusion in the presence of calcein as used previously [6]. The progressive leakage of the dye was followed through the decrease in the fluorescence intensity at 505 nm under stirring at 25°C after dropwise addition of defined amounts of peptides. That decreased intensity resulted from the total quenching of the released calcein by external Co^{2+}, $[Co^{2+}] = 0.25$ mM, [46]. The total release of calcein was assessed by Triton X-100 addition at the end of the process induced by the peptide.

2.5. Fluorescence spectroscopy

Emission spectra of peptides were obtained on a Fluoromax spectrofluorimeter from Spex. Spectra of buffer as well as buffer with lipids were subtracted from sample spectra to eliminate Raman and light scattering contributions. The degree of fluorescence polarization, P, was obtained on a SLM 8000 spectrofluorometer modified to automatically record I_v, I_h alternately. The polarization values were averaged over seven acquisitions of I_v and I_h measured for 40 s. The temperature was maintained at 25 or 20°C by Peltier devices and the solutions were stirred with a magnetic device [6].

2.6. Film formation and surface pressure measurements

The experiments were performed on a computer-controlled Langmuir film balance (Nima Technology, Coventry, UK). The rectangular trough (110 cm^3, 145 cm^2) and the barrier were made of teflon. The surface pressure (Π) was measured by the Wilhelmy method using a filter paper plate. Troughs were filled with an aqueous buffer (20 mM Tris, 130 mM NaCl, HCl, pH = 7.5) using ultra pure water (Milli-Q, Millipore). The experiments were carried out at 25 ± 2°C. A few μl of MeOH peptide stock solutions was always injected into the subphase to define the total peptide concentrations.

To obtain mixed peptide/DMPC films, pure DMPC was spread at the air/water interface from chloroform solutions using a Hamilton microsyringe until low lateral pressures (≈2–3 mN/m) were reached. At pressure equilibrium, i.e. after ≈15 min, the phospholipid film was slowly compressed (5 cm^2/min) up to 30 mN/m. In a second step, a few μl of concentrated peptide solutions was injected into the subphase and the surface increases (ΔS) was recorded for each peptide concentration after 30–40 min.

2.7. FT-IR spectroscopy measurements

Absorbance spectra of pure peptides as bulk samples were obtained by conventional transmission spectroscopy after a methanolic solution was evaporated on a ZnSe window.

Interface study of peptides and mixed peptide/DMPC monolayers was done in situ by PMIRRAS [39,40]. The spectra were recorded on a Nicolet 740 spectrometer equipped with a HgCdTe detector cooled at 77 K. Generally, 200 or 300 scans were pooled at a resolution of 4 or 8 cm^{-1} for pure peptide or mixed peptide/DMPC monolayers, respectively. Briefly, PMIRRAS combines FT-IR reflection spectroscopy with fast polarization modulation of the incident beam between parallel (p) and perpendicular (s) polarization. Two-channel processing of the detected signal allows us to obtain the differential reflectivity spectrum:

$$\Delta R/R = [(R_p - R_s)/(R_p + R_s)]J_2$$

To remove the contribution of liquid water absorption and the dependence on Bessel functions J_2, the monolayer spectra are divided by that of the subphase. With an incidence angle of 75°, transition moments preferentially oriented in the plane of the interface give intense and upward oriented bands, while perpendicular ones give downward oriented bands.

The decomposition of the amide I and amide II spectral region (1500–1800 cm^{-1}) into individual bands was performed with the Peaksolve (version 3.0, Galactic) software and analyzed as a sum of Gaussian/Lorentzian curves, with consecutive optimization of amplitudes, band positions, half-width and Gaussian/Lorentzian composition of the individual bands.

2.8. Calculations of the peptide hydrodynamic volume by the Perrin equation

The degree of polarization, P, of a fluorescent group is related to the dynamics of the molecule, according to the Perrin equation [47]:

$$\left(\frac{1}{P} - \frac{1}{P_0}\right) = \left(\frac{1}{P_0} - \frac{1}{3}\right)\left(1 + \frac{RT\tau}{\eta V_h}\right)$$

where T = absolute temperature, η = viscosity of the medium, τ = fluorescence lifetime, V_h = hydrodynamic volume of the fluorophore and P_0 = fundamental degree of polarization. For the Dns-labelled $(KL)_7K$ peptide, the graph $P^{-1} = f(T/\eta)$ was plotted through changes on the viscosity of the solution, η, by successive glycerol additions at 298 K. The hydrodynamic volume of the peptide, V_h^{exp}, was estimated from the slope of the linear plot,

$$s = \left(\frac{1}{P_0} - \frac{1}{3}\right)\frac{RT\tau}{V_h}$$

and the independent measurement of τ. This value was compared to the calculated hydrodynamic volume of a monomeric $(KL)_7K$, V_h^{mono}:

$$V_h^{mono} = \frac{M}{N_{av}}(V_2 + \delta V_1^0)$$

where V_2 is the partial specific volume of the peptide,

$$V_2 = \frac{\sum_1^n n_i w_i V_i}{\sum_1^n n_i w_i}$$

(w_i, V_i) are, respectively, weight and specific volumes of the amino acid i [48] and (236 g/mol, 0.74 cm^3/g) for the Dns; $V_1^0 \approx 1$ cm^3/g = specific volume of solution; M = peptide molecular weight; $N_{av} = 6.02 \times 10^{23}$; δ = hydration degree. For native globular proteins, $\delta = 0.3$ g/g [49], but it could be higher for other protein shapes (1–2 g/g) [50].

2.9. Estimate of the partition coefficients from the aqueous solution to the lipid monolayer

A partition constant, K_{aff}^{30}, for the transfer of the peptide from the aqueous solution to the lipid monolayer compressed at 30 mN/m can be extracted from the plots $\Delta S/S_0 = f(c)$. The classical definition for a peptide/bilayer interaction is used [7,51]:

$$K_{aff}^{\Pi} = \frac{C_b^p}{C_f^p \times C_L^0}, \text{ with } C_b^p = \frac{\Delta S}{S_{mol} N_{Av} V},$$

$$C_L^0 = \frac{S_0}{A_L^{\Pi} N_{Av} V} \text{ and } C_f^p = C_{total}^p - C_b^p$$

C_b^p, the concentration of bound peptide in the total subphase volume (110 ml), is estimated from the measured surface increase, ΔS, assuming that (i) the total surface results from additivity rules and (ii) the molecular surface of each compound at the interface is constant throughout the binding process. S_{mol} is the peptide molecular surface, N_{av} is the Avogadro number.

Table 1
Names, sequences and physico-chemical characteristics of the peptides studied

Name	Composition	molecular weight (g/mol)	net charge	sequence
				1 4 8 11 15
$(KL)_4K$	L4K5	1344	+5	Dns-K L K L K L K L K-$CONH_2$
$(KL)_5K$	L5K6	1585	+6	Dns-K L K L K L K L K L K-$CONH_2$
$(KL)_6K$	L6K7	1826	+7	Dns-K L K L K L K L K L K L K-$CONH_2$
$(KL)_7K$	L7K8	2067	+8	Dns-K L K L K L K L K L K L K L K-$CONH_2$
i.a.DnsLK_{15}	L10K5	2026.5	+4	Dns-K L L K L L L K L L L K L L K

C_L^0, the lipid concentration with respect to the total subphase volume (110 ml) is calculated as S_0/A_L^{Π}, the ratio of the initial surface of spread DMPC to the molecular area of DMPC at 30 mN/m ($A_L^{30} = 60$ Å^2 [52]).

C_f^p, the concentration of free peptide in the subphase.

The relation between K_{aff}^{Π} and the slopes P_p^{Π} of the $\Delta S/S_0 = f(c)$ plots is then defined as:

$$K_{aff}^{\Pi} = P_p^{\Pi} \times \frac{C_{total}^P \times \frac{A_L^{\Pi}}{S_{mol}}}{\left(C_{total}^P - \frac{\Delta S}{S_{mol} N_{Av} V}\right)}$$

3. Results

3.1. Design of amphipathic peptides

The $(KL)_mK$ peptides of 4 to 7-mer in length were designed to generate ideally amphipathic β-sheets, they have a L/K = 1 ratio and a strict 2-fold periodicity throughout the sequence (Table 1). The increase in length from 9 to 15 residues, when a (KL) motif was added, led to a regular increase in net charge from +5 to +8. Their hydrophobic moment, μ_H, which is a quantitative estimate of amphipathicity, was estimated using the consensus scale of hydrophobicity [53]. Maximal values were obtained for the β-sheet structure, with a linear increase of μ_H^{β} from 7.6 to 12.5 when the peptide length increased from 9 to 15 residues.

To check for a real progressive increase in amphipathicity in the series, the affinity of the peptides for C_{18} chains of a RP-HPLC column was assayed and their RT were measured [54]. The four peptides studied eluted for a similar CH_3CN gradient (44 ± 1%) at very short RT, thus confirming their high hydrophilicity and relatively low affinity for the stationary phase. The good linear correlation be-

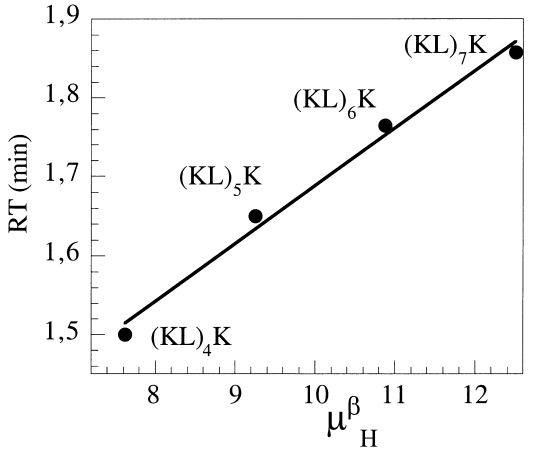

Fig. 1. Calculated total hydrophobic moment, μ_H^{β}, of the $(KL)_mK$ peptides (m = 4–7) versus experimental RT on a C_{18} column by RP-HPLC eluted with a CH_3CN gradient. The straight line corresponds to correlation factor R = 0.995.

tween RT values and μ_H^β (Fig. 1) showed that the peptides eluted in the order expected for increasing their total hydrophobicity, i.e. their L content.

3.2. Peptide behavior in aqueous solution

All $(KL)_mK$ peptides studied had a dansyl group at the N-terminus. They displayed similar fluorescence emission parameters in aqueous Tris buffer with $\lambda_{max}^{em} = 547 \pm 1$ nm and $I_{max}^{em} = 0.16 \pm 0.03$. These values are very close to those of DnsK, which was used as reference for a Dns totally exposed to the solvent: $\lambda_{max}^{em}(DnsK) = 546$ nm and $I_{max}^{em} = 0.17 \pm 0.02$. Whatever the peptide, their low polarization degree, $P = 0.075 \pm 0.010$, pointed to a high mobility of the Dns. The hydrodynamic volume, V_h^{exp}, of $(KL)_7K$ was estimated using the Perrin isotherm (Fig. 2). The slope of the linear plot and the independent measurement of the Dns fluorescence lifetime, $\tau \approx 3.8$ ns (data not shown), gave $V_h^{exp} \approx 4110$ Å^3, in agreement with the theoretical hydrodynamic volume for a monomeric $(KL)_7K$, 3925 Å$^3 < V_h^{mono} < 6331$ Å^3, according to hydration degrees (0.3–1 g/g). Therefore, the longest peptide was monomeric in aqueous solution. As this was the most hydrophobic of the series, all the peptides were thus monomeric in aqueous solution at the low concentrations used here (2 μM).

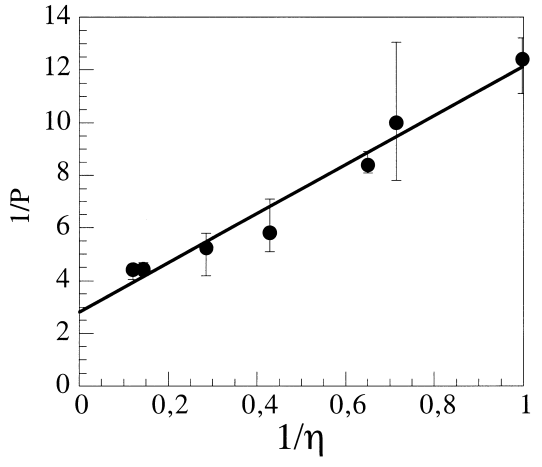

Fig. 2. Dns fluorescence polarization degree of peptide $(KL)_7K$ in solution. Perrin plot, $1/P = f(1/\eta)$, P is the polarization degree and η the viscosity of the medium. $[(KL)_7K] = 2$ μM, $T = 20$°C, 20 mM Tris–HCl, pH = 7.5 buffer. η was progressively increased by glycerol additions. The straight line corresponds to correlation factor $R = 0.994$.

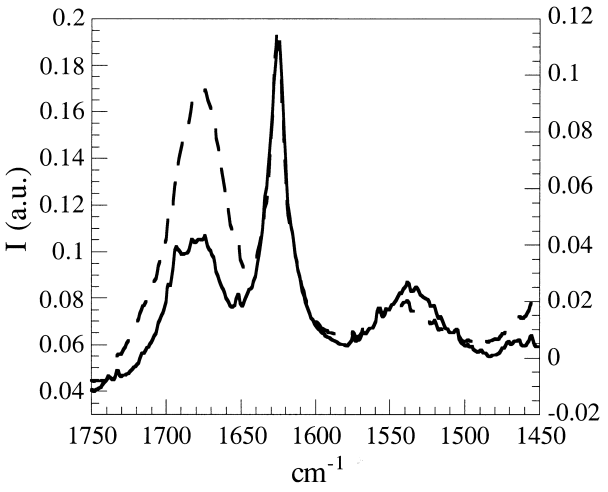

Fig. 3. IR absorption spectra in bulk state for the amide vibration domain: dashed line $(KL)_4K$, line $(KL)_7K$.

3.3. Peptide structure by FT-IR and PMIRRAS

FT-IR absorption spectra of $(KL)_4K$ and $(KL)_7K$ in the bulk solid state display a very sharp and intense amide I band around 1625 cm^{-1} which was attributed to β-sheets (Fig. 3). The strongest one around 1677 cm^{-1} is mainly due to β-turns [55–57] but can also contain a weak contribution of the TFA counter ions used for purification [56]. The deconvolution of the spectra of all the peptides (Table 2) confirms the major contributions of β-turns and β-sheets. The band around 1625 cm^{-1} is well fitted by three components at 1632, 1626 and 1615 cm^{-1}, which likely represent the split amide I vibrational mode of a mixture of parallel (1632 cm^{-1}) and antiparallel β-sheets (1626 and 1615 cm^{-1}) [55–60]. The weak contribution around 1694 ± 1 cm^{-1} also characterizes antiparallel β-sheets and some random structures around 1650 cm^{-1} are present on the $(KL)_6K$ and $(KL)_7K$ spectra (Table 2). The amide II mode absorbs around 1544 cm^{-1}. The band around 1625 cm^{-1} sharpens in parallel to the peptide length increase and the relative proportion of β-sheets increases to become highly predominant (Table 2).

The peptides formed films at the air/water interface (see below) and their in situ PMIRRAS spectra display similar shapes (Fig. 4). The major amide I band, split into two components around 1622 cm^{-1} (A_I) and 1694 cm^{-1} ($A_{I'}$), characterizes a quasi-pure

Table 2
Frequencies and band assignments in the amide I domain for deconvoluted IR mass spectra of $(KL)_nL$ peptides

Peptide	cm^{-1}	Relative area (%)	Band width (cm^{-1})	Assignment
$(KL)_4K$	1693	1	6.5	β-Sheet
	1677	77	35.0	β-Turn (+TFA)
	1632-1613	22	31-13	β-Sheet
$(KL)_5K$	1690	1.1	17	β-Sheet
	1677	54.8	38	β-Turn (+TFA)
	1627	44.1	25	β-Sheet
$(KL)_6K$	1693	7.6	14.8	β-Sheet
	1678	32.1	38.0	β-Turn (+TFA)
	1650	5.8	17.1	Random
	1632-1626-1616	54.4	14.2-10.2-16.9	β-Sheet
$(KL)_7K$	1695	9.7	14.7	β-Sheet
	1676	29.0	28.5	β-Turn (+TFA)
	1650	3.2	15.6	Random
	1632-1626-1613	58.1	18.9-11.6-12.2	β-Sheet

folding into β-sheets. The contributions of the β-turns and random structures now vanish, which is indicative of a strict β-structure induced by the interface. The spectra registered for two different compression states of the films show that the absorption frequencies are lateral pressure-independent in the 1–20 mN/m and 15–25 mN/m domains for the 9- and 15-mer, respectively (Fig. 4).

The peptides also insert into compressed DMPC monolayers spread at the air/water interface. On all the in situ PMIRRAS spectra (Fig. 5), the characteristic lipid absorption bands of DMPC: $\nu_{c=0}^{ester}$ around 1730 cm^{-1}, δ_{CH2} around 1470 cm^{-1} and $\nu_{P=0}^{antisym}$ around 1225 cm^{-1}, which are intense and well defined for the pure DMPC film at 30 mN/m, decreased in intensity when the peptides were inserted in the monolayer. In the mixed peptide/DMPC films, the amide I mode is split into a very sharp intense A_I band ($\approx$1622 cm^{-1}) and a weaker $A_{I'}$ one ($\approx$1693 cm^{-1}), characteristic of peptide antiparallel β-sheets in the lipid environment. Similar data were obtained for the 11- and 13-mer (spectra not shown). Therefore, whatever the experimental conditions, all the peptides folded into antiparallel β-sheets.

3.4. Peptide orientation in situ by PMIRRAS

PMIRRAS spectra also gave information about the peptide orientation at the interface. With the experimental set-up used, absorption transition moments in the plane of the interface give strong upward-oriented bands, while perpendicular ones give medium and/or downward-oriented bands [40]. Since all the $(KL)_mK$ peptides form antiparallel β-sheets at the interfaces, simulations were performed using a general software program to estimate their orientation [61]. The optical anisotropic index of the films was generated by taking into account the infra-red (IR) absorptions and dichroism for amide I′ (1685 cm^{-1}), amide I (1625 cm^{-1}) and amide II domains measured on spectra of pure β-sheeted peptides and using the optical anisotropic index of water [62]. Briefly, the β-sheet structure can be considered as a two-dimensional unit cell with two reference axes corresponding to the average orientations of the amide I′ and amide I transition moments. The amide I′ (1685 cm^{-1}) transition moment is oriented along the peptidic chain while the amide I (1625 cm^{-1}) one, perpendicular to the former, corresponds to interchain hydrogen bonds. In the bulk state, the relative intensity ratio is $I_{AI(1626\ cm^{-1})}/I_{AI'(1685\ cm^{-1})} \sim 10$. Another amide I transition moment ($A_{I''}$) absorbs around 1670 cm^{-1} and is perpendicular to the β-sheet plane but its intensity is much weaker ($I_{AI(1625cm^{-1})}/I_{AI''(1670cm^{-1})} \sim 20$) [55,63], so it was not introduced in the simulations. According to the selection rules at the air/water interface and for the three following extreme orientations, it results that (i) a β-sheet flat oriented at the interface plane gives a weak positive amide I′ (1685 cm^{-1}) band and a strong positive amide I (1625 cm^{-1}) one; $I_{AI}/I_{AI'} \sim 9$ is then close to what is observed in the

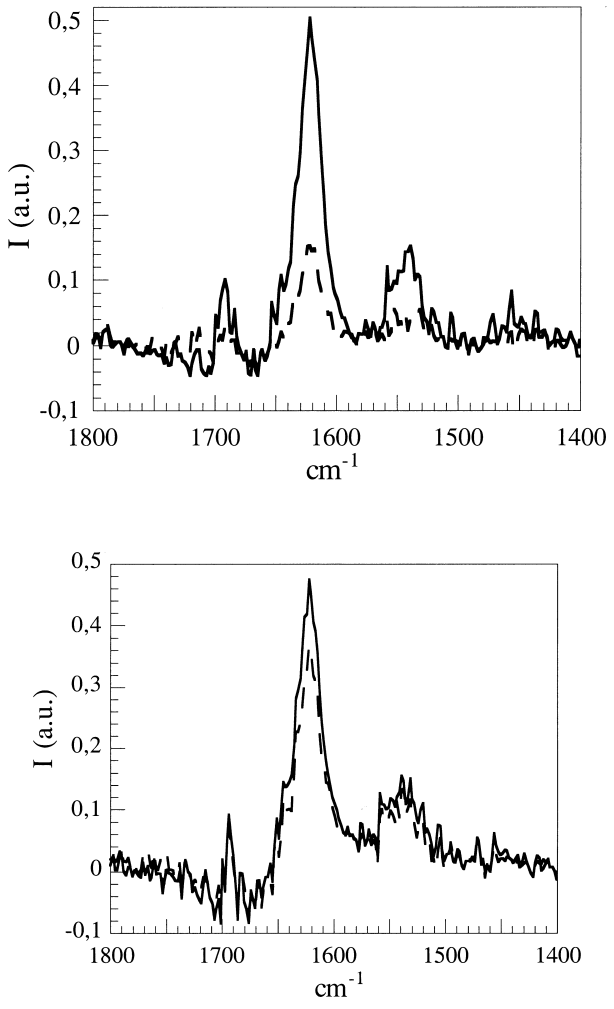

Fig. 4. PMIRRAS spectra of pure peptidic films in situ at the air/water interface at different lateral pressures, Π: a (top): $(KL)_4K$ (62.2 nM): dashed line $\Pi = 1$ mN/m, line $\Pi = 20$ mN/m; b (bottom): $(KL)_7K$ (20 nM): dashed line $\Pi = 15$ mN/m, line $\Pi = 25$ mN/m. Subphase: 20 mM Tris, 130 mM NaCl, HCl, pH = 7.5, $T = 25$°C.

bulk state, (ii) a β-sheet oriented perpendicular to the interface with the peptidic chains parallel to the interface gives a positive amide I′ band and a strong negative amide I one, (iii) a β-sheet perpendicular to the interface with the direction of the peptidic chains perpendicular to the interface plane gives a negative amide I′ band and a strong positive amide I one.

PMIRRAS spectra of the $(KL)_4K$ and $(KL)_7K$ at the air/water interface and inserted in the DMPC monolayer (Figs. 4 and 5) display a positive, very sharp strong band around 1622 cm^{-1} and another positive one around 1693 cm^{-1}, both indicative of transition moments oriented in the interface plane. The high values of the intensity ratios $I_{AI(1622\,cm^{-1})}/I_{AI'(1693\,cm^{-1})} > 8$ at the air/water interface and > 6 in the DMPC monolayer characterize antiparallel β-sheets flat-oriented or slightly tilted at the interface, whatever the peptide. Furthermore, at the air/water interface, this ratio remains constant whatever the compression state, so the flat orientation is also lateral pressure-independent.

From such structure and orientation conclusions, a molecular area for each peptide at the interface, S_{mol}, can be estimated: an antiparallel β-sheet parallel to the interface plane occupies $n \times 3.4$ Å $\times 4.7$ Å $= 16 \times n$ Å^2, where n is the number of residues [64–67]. Adding 80 Å^2 to account for the Dns group led to 226, 256, 288 and 320 Å^2 for the $(KL)_4K$, $(KL)_5K$, $(KL)_6K$ and $(KL)_7K$, respectively.

3.5. Surface activity and affinity for a DMPC monolayer

When a few μl of the peptide stock solutions was injected in the subphase, significant surface pressure changes indicated the surface activity of the peptides, as previously shown by obtaining the pure peptidic films at the air/water interface used for the PMIRRAS in situ study (Fig. 4). All peptides were highly

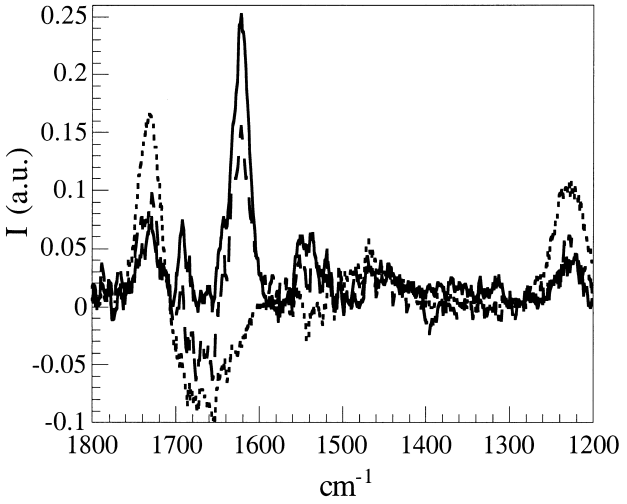

Fig. 5. In situ PMIRRAS spectra of peptides inserted into a DMPC monolayer at constant pressure, $\Pi = 30$ mN/m: dotted line, pure DMPC; line, mixed $(KL)_4K$ (60 nM)/DMPC; dashed line, mixed $(KL)_7K$ (40 nM)/DMPC. Subphase: 20 mM Tris, 130 mM NaCl, HCl, pH = 7.5, $T = 25$°C.

surface-active and formed densely packed films at the interface. The films were stable up to their collapse pressures, Π_{coll}, which could be up to 30 mN/m (data not shown).

The lipid affinity of the peptides was monitored by measuring the area increase of a pre-formed lipid monolayer at constant surface pressure [51] using $\Pi = 30$ mN/m to mimic lipid bilayers or biological membranes [68]. Peptide injection in the subphase led to surface increases and the changes in the relative area of the mixed peptide/lipid films ($\Delta S/S_0$) versus the total peptide concentration (c) (Fig. 6) show that, in the concentration range of 10^{-8}–2×10^{-7} M, all the peptides were inserted in the DMPC monolayer. The experimental data are well fitted by linear plots (Fig. 6). Their slopes, P_p^{30}, monotonically increase in parallel with the peptide length: 114 ± 5, 200 ± 5, 233 ± 5 and 508 ± 5 μM^{-1} for the 9-, 11-, 13- and 15-mer, respectively. They are proportional to the number of peptide molecules in the film, i.e. related to their partition coefficient, K_{aff}^{30}, between the DMPC monolayer and the aqueous phase and to the molecular surface for each peptide at the interface, S_{mol}, (see above). Estimates of K_{aff}^{30} give $\approx0.33\times10^6$ M^{-1} for the $(KL)_4K$, $\approx0.53\times10^6$ M^{-1} for the $(KL)_5K$, $\approx0.54\times10^6$ M^{-1} for the $(KL)_6K$ and $\approx1.18\times10^6$ M^{-1} for the $(KL)_7K$, so lipid affinity increases with peptide length.

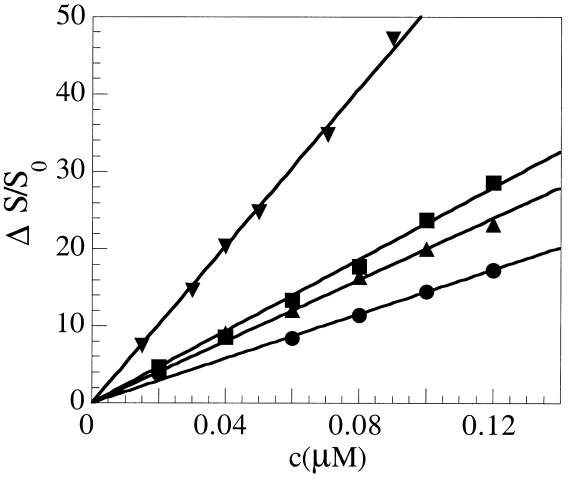

Fig. 6. Relative film surface increases due to peptide insertion at constant pressure, $\Pi = 30$ mN/m, in pre-formed DMPC monolayers for the $(KL)_mK$ peptides ($m = 4$–7) on increasing their bulk concentration in the subphase: ● $(KL)_4K$, ▲ $(KL)_5K$, ■ $(KL)_6K$, ▼ $(KL)_7K$. Subphase: 20 mM Tris, 130 mM NaCl, HCl, pH = 7.5, $T = 25$°C.

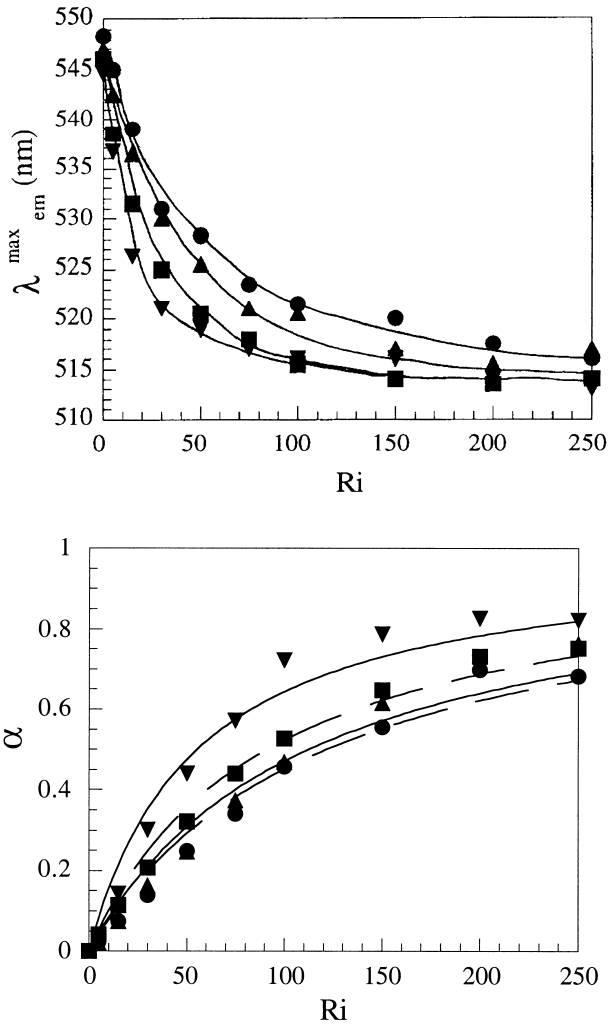

Fig. 7. Interaction of $(KL)_mK$ peptides ($m = 4$–7) with EPC-Chol (20/1 ratio) SUVs as followed by changes in the Dns emission parameters versus R_i, the lipid to peptide molar ratio. a (top): Changes in the emission maximum wavelength of the dansyl group, λ_{max}^{em}. b (bottom): Changes in the fraction of bound peptide, α, as estimated from fluorescence intensity changes at 510 nm. Lines are the best fits according to the peptide partition. ● $(KL)_4K$, ▲ $(KL)_5K$, ■ $(KL)_6K$, ▼ $(KL)_7K$. Peptide concentrations = 2 μM, $\lambda_{exc} = 340$ nm, Tris 20 mM, pH 7.5 buffer, $T = 25$°C.

3.6. Interaction with EPC-Chol (20/1 ratio) SUVs and affinity for bilayers as followed by fluorescence

To validate the results obtained on DMPC mono-

layers, peptide interactions with lipids were monitored by fluorescence for successive additions of EPC-Chol (20/1 ratio) SUVs to increase the lipid to peptide molar ratio, R_i. For all the peptides of the series, the initially exposed Dns with an emission maximum at $\lambda_{max}^{em} \approx 547 \pm 1$ nm was similarly and progressively buried to $\lambda_{max}^{em} = 517 \pm 2$ nm for $R_i = 150$ (Fig. 7a) and the fluorescence intensity was increased to $\Delta I/I_0 = 50\%$. Whatever the length from 9 to 15 residues, low Dns fluorescence polarization values, $P = 0.075 \pm 0.01$, were obtained for the peptides free in buffer. On lipid addition, very significant increases gave a similar average value, $P = 0.188 \pm 0.012$ at $R_i = 150$, but P remained weaker than $P_0 \approx 0.33$ obtained for a totally immobilized fluorophore. Therefore, all the $(KL)_mK$ peptides bound to the lipid vesicles with a burying of their N-terminus and a restricted Dns motion. Very similar fluorescence parameters in the presence of a lipid excess indicated a similar Dns location whatever the peptide length.

The characteristic change in intensity for totally bound peptides was extrapolated from a double reciprocal plot of $I_{em}^{510\ nm}$ versus R_i and the fraction of bound peptide (α) was quantitatively defined throughout the binding curves (Fig. 7b). The experimental data were fitted with the simple model of partition between two phases: the aqueous one and the lipidic one in vesicles [69]. The partition constant, K_p, defined as the ratio of the peptide concentration in both phases, monotonically increased throughout the series from 5.2×10^3, 5.6×10^3, 7.7×10^3 and 11.4×10^3 for $(KL)_4K$, $(KL)_5K$, $(KL)_6K$ and $(KL)_7K$, respectively. Thus, the affinity for the lipidic phase increased with the length.

3.7. Lytic activity

Since the peptides interact with zwitterionic lipids, their ability to induce an increase in bilayer permeability was monitored as usually by looking at the induced calcein dye escape from LUVs [6]. The same lipid mixture as already used in the binding study was used, it is assumed to mimic the composition of the outer leaflet of erythrocytes [70,71]. In the μM concentration range, peptides induced a fast decrease in the dye fluorescence intensity indicative of significant leakages of calcein due to their quenching by the external cobalt. A few minutes after peptide addition, a plateau is observed. This indicates the recovery of a non-permeant state of the vesicles (Fig. 8a). On increasing the peptide concentration, the % of leakage increased up to total escape for a very high peptide concentration. For the longer peptide, $(KL)_7K$, 50% escape was observed at $R_i \approx 13$, i.e. for very larger peptide amounts compared to the i.a. DnsLK15 [6].

The dose-response curves of hemolysis on human erythrocytes (Fig. 8b) showed that all the peptides displayed quite similar sigmoidal curves with total lysis observed for concentrations < 30 μM. The concentrations required for 50% lysis, LD_{50} values, regularly decreased versus peptide length: $LD_{50} \approx 22$, 8,

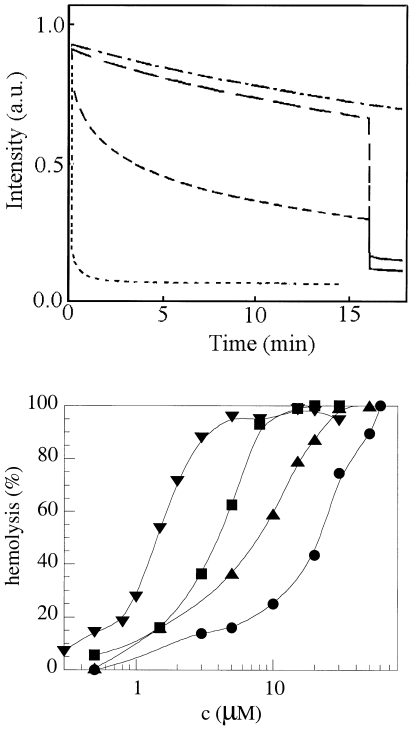

Fig. 8. Lytic activity of the studied $(KL)_mK$ peptides. a (top): Kinetics of the calcein leakage, when trapped inside EPC-Chol (20/1 molar ratio), after peptide addition at $t = 0$, in the presence of 0.25 mM external cobalt concentration. The total leakage was induced by Triton X-100 addition at $t = 18$ min. Permeability increase induced at different R_i values: — — $R_i = 130$; — — — $R_i = 13$; dotted line $R_i = 1.3$; —•— = passive permeability of LUVs alone. b (bottom): Dose-response plots of human red blood cell hemolysis induced by the $(KL)_mK$ peptides ($m = 4$–7). ● $(KL)_4K$, ▲ $(KL)_5K$, ■ $(KL)_6K$, ▼ $(KL)_7K$. 10^7 cells per ml in 20 mM Tris, 130 mM NaCl, HCl, pH = 7.5 buffer after 30 min at 37°C.

4 and 1.5 μM for $(KL)_4K$, $(KL)_5K$, $(KL)_6K$ and $(KL)_7K$, respectively.

4. Discussion

4.1. Peptide design, secondary structure and orientation at the interfaces

With a 1/1 L to K composition and a strict 2-fold periodicity throughout the sequence, $(KL)_mK$ peptides ($m = 4$–7) were designed to generate ideally amphipathic basic β-sheets. That really occurs as shown by PMIRRAS in situ at the air/water interface for both pure peptide and mixed peptide/DMPC films. These latter displayed main peptide amide I absorption modes characteristic of antiparallel β-sheet structures [55–57]. Furthermore, this structure was preserved whatever the lateral pressure applied. Therefore, as expected from their design and from the high values calculated for the hydrophobic moment μ_H^β, all the $(KL)_mK$ studied peptides fold into ideally amphipathic antiparallel β-sheets with a strict clustering of the charged K residues on one face while the opposite face is constituted by only L residues. Their β-strands length increases from ∼31.5 to ∼50 Å in the direction of the peptidic chain. These conclusions agree totally with those previously obtained for a short seven residues long $Fmoc(LK)_3K$ peptide in Langmuir–Blodgett-transferred monolayers of pure peptide [36] and for a 18 residues long $(KL)_9$ peptide studied by CD when bound to C_{18}-coated quartz plates assumed to mimic the membrane environment [37]. They also agree with the conclusions of the study of $(KV)_n$ peptides, despite that these latter only interact significantly with charged lipids, probably due to a lower hydrophobicity [31].

PMIRRAS spectra of the peptides alone or inserted into a DMPC monolayer made it possible to conclude that the β-sheet orientation remains flat whatever the lateral pressure applied and the peptide length. Such an interfacial orientation is cogent with the fact that β-sheets of the longer peptides (≥11 residues) would be too long to stabilize the unfavorable hydrophilic/hydrophobic interactions with a transmembraneous orientation in a bilayer core, unless they were severely tilted. This also rules out, very probably, the occurrence of β-barrel structures as observed in soluble [72] or membrane proteins [73].

Furthermore, when bound to EPC SUVs, all the $(KL)_mK$ peptides displayed very similar Dns fluorescence emission parameters, which reflected similar Dns location and dynamics. Plotted on an abacus versus the dielectric constant of the solvent (data not shown), λ_{em}^{max}(Dns) in the bound state characterizes a burying of the N-terminus of all the peptides in a still polar position, i.e. not deeply inserted in aliphatic chains. Very similar locations have been found when the Dns is covalently bound to the N-terminus of L_iK_j α-helical peptides and to Q_{25}melittin in interaction with lecithin vesicles [6,44]. Such fluorescence conclusions totally agree with the PMIRRAS data on monolayers and strongly support a flat-oriented peptide on the external leaflet of the vesicles. Similar molecular orientations without deep penetration into the membranes were also proposed for other β-sheeted toxins: $(SVKV)_n$ and $(KV)_n$ peptides [31], a linear analog of tachyplesin I [23], natural cardiotoxins [14], lactoferricin B [25] and truncated pardaxin analogues [70]. However, the exact positioning of β-sheeted structures within membranes remains an open and important problem. In order to be addressed, it first requires to better define the number of strands and the type of 'motif' on folding. The relative positions of β-sheeted peptides and lipids could also be modulated by peptide-bound concentration and physico-chemical constraints in buffer and in the membrane, as now recognized for α-helical peptides [74]. This will indeed deserve more attention.

4.2. Behavior of peptides in solution and affinity for the interfaces (air/water, phospholipid mono- and bilayers)

In solution, the $(KL)_mK$ peptides eluted on RP-HPLC, as expected from the linear increase of their length and their hydrophobic moment. Furthermore, at comparable length, these highly charged peptides from +5 to +8 eluted at shorter RT compared to L/K = 2 peptides [6]. Therefore, under good solvent conditions, hydrophobicity and amphipathicity are critical parameters which modulate peptide affinity for the hydrophobic stationary phase. In aqueous solution, the fluorescence parameters of all the pep-

tides and the hydrodynamic volume of the 15-mer indicated a monomeric state, whatever their length.

These conclusions agree with those on other compounds with 1/1 apolar to polar residues [36], but also with our previous finding of a monomeric form of KLLLKLLLK, i.e. the nine residues long LK peptide analogous to $(KL)_4K$ but with a 2/1 L/K ratio and which is also β-sheeted when bound [6,7]. However, in this last series, designed to generate ideally amphipathic α-helices, a self-association process concomitant with length increase was demonstrated [6]. So, the low L/K = 1 ratio, which implies a lower hydrophobicity, and the strong electrostatic repulsive effect ensure good solubility in aqueous buffer. The 15-mer peptide which is monomeric under the experimental conditions used herein should oligomerize at higher concentrations and/or ionic strengths.

Therefore, under the conditions used herein, all the peptides displayed the same initial monomeric state in solution and common oligomeric β-sheeted structures and orientation when bound to lipids. This allows us to compare the evolution of the affinities for various interfaces. Due to their high amphipathic character, all the $(KL)_mK$ peptides formed stable films at the air/water interface and were significantly surface-active. These results are closely related to those obtained for the $Fmoc(LK)_3L$ [36] and with the L_iK_j peptides which have a 3.6 periodicity [7]. At the same length, the collapse pressure of the $DnsKL_3KL_3K$ folded into pure β-sheets [7] was about 5 mN/m lower than that of the $(KL)_4K$. Then, the stability of the films depends on their ideal amphipathicity and not on their total hydrophobicity. Longer peptides, such as $DnsLK_{15}$ ($DnsKL_2KL_3KL_3KL_2K$) and $(KL)_7K$, display similar surface activity ($\Pi_{coll} = 36 \pm 1$ mN/m) despite that they fold into α-helix and β-sheet, respectively [7,38]. Therefore, it is the ideal amphipathic character of the peptides and neither the type of secondary structure nor the L/K ratio which are preponderant for the surface activity.

The high surface activity allows for these peptides to insert in DMPC monolayers spread at the interface. The strict linear increase in the film area versus peptide concentration could mean ideal mixing of the two partners or at the opposite phase separation in the film. The partition constants, K_{aff}^{30}, from the subphase to the compressed monolayer regularly increased with peptide length, in agreement with the RP-HPLC data under good solvent conditions. The clear correlation between the hierarchies of affinity determined on lipid mono- and bilayer model systems (Fig. 9) confirms that the monolayer system is particularly well suited for such a lipid affinity study [51]. This also justifies retrospectively the approximations done to interpret the ΔS changes and validates the extrapolation to bilayers of the secondary structure and orientation conclusions obtained by PMIRRAS.

Therefore, in this $(KL)_mK$ series, the lipid affinity for zwitterionic lipids is mainly driven by the hydrophobic effect. Moreover, when compared with the affinities obtained for the monomeric short LK peptides with a L/K = 2 ratio, the lipid affinity of the

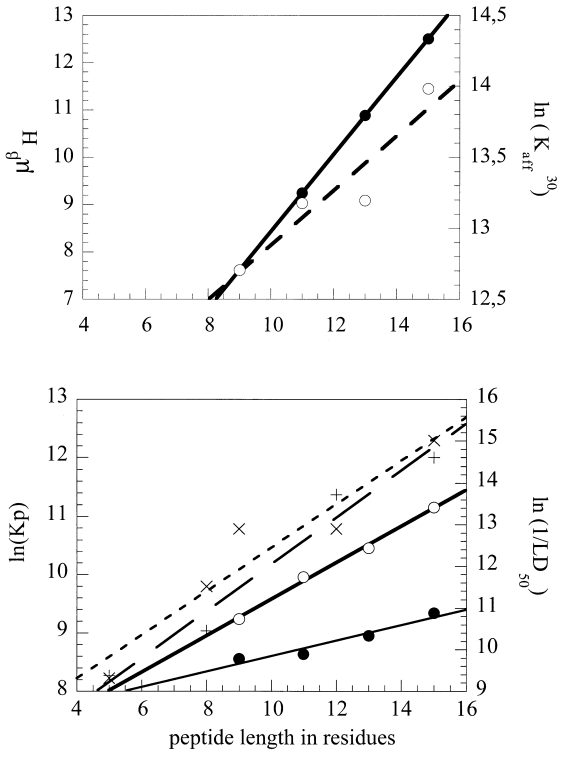

Fig. 9. Plots of different properties of the amphipathic $(KL)_mK$ and L*i*K*j* peptides versus peptide length: a (top): (●) Hydrophobic moment, μ_H^β, calculated for a β-sheet folding [7,78], $R = 0.998$; (○) affinity for a DMPC monolayer compressed at 30 mN/m, K_{aff}^{30}, $R = 0.940$. b (bottom): Affinity for EPC-Chol (5%) SUV bilayers, K_p, for $Dns(KL)_mK$ (●), $R = 0.984$ and for $(Dns)L_iK_j$ ($i = 2j$) (+), $R = 0.965$. Hemolytic activity, $1/LD_{50}$, for $Dns(KL)_mK$ (○), $R = 0.997$ and for $(Dns)L_iK_j$ ($i = 2j$) (×), $R = 0.954$. [7,78]. R: correlation factor.

$(KL)_mK$ at comparable length (<13 residues) is more than an order of magnitude lower on the same lipid systems [6,7]. Even the $DnsLK_{15}$, which is strongly self-associated in solution, had a greater affinity for mono- and bilayers than the monomeric $(KL)_7K$. Indeed, the decrease in the relative L content, which parallels the better water solubility of the peptides, considerably reduces their lipid affinity. This totally agrees with conclusions reached for α-helical peptides [75,76].

A free energy of transfer from the aqueous phase to the lipid one, ΔG_{ins}, was extracted from the fit of experimental data by a straight line. From its slope and using the equations $\Delta G_{ins} = -RT\ln(55.5 \times K_{aff}^{30})$ or $-RT\ln(K_p)$, the average contribution per (LK) unit is roughly the same for both lipid systems, -0.20 ± 0.05 kcal/mol. The absolute value is significantly lower than the 1.19 kcal/mol calculated by simple additivity of the free energy of transfer for the L and K residues from the aqueous phase to an apolar medium [77]. Though the fact that an absolute comparison is very difficult since the experimental conditions are different, these results indicate that peptide affinity is also modulated by other and more complex criteria than the hydrophobicity alone. The comparison of $(KL)_7K$ and $DnsLK_{12}$, ($DnsKL_3KL_3KL_2K$), which are respectively folded into β-sheet and α-helix in the bound state [7,78] but have almost the same L content (seven and eight, respectively), shows that the affinity of the β-sheeted $(KL)_7K$ is lower both for DMPC monolayers ($\approx$9-fold) and for EPC bilayers ($\approx$6-fold). This could be due to the very different hydrophilic contributions imposed by their composition (eight K for the $(KL)_7K$ and only four for the $DnsKL_{12}$) and/or due to an intrinsic difference between α- and β-structures. This has already been suggested from the comparison of two 18 residues long LK peptides with the same composition: the ideally amphipathic $(KL)_9$ with a 2-fold symmetry displayed a lower affinity for LPC and C_{18}-coated plates than the ideally amphipathic one with a 3.6-fold symmetry [37].

4.3. Correlations with hemolytic activity

Due to their ideally amphipathic character and their affinity for zwitterionic lipids, the $(KL)_mK$ peptides displayed a significant hemolytic activity. With lethal doses in the 1.5–22 μM range, they are probably the most hemolytic β-sheeted peptides studied until now despite that they are shorter than all the natural β-sheeted peptides, out of the cyclic decapeptide gramicidin S. All such natural hemolytic β-sheeted compounds are either cyclic or stabilized by intramolecular disulfide bridges [18–21,23]. Therefore, large β-sheets cannot be formed unless oligomerization occurs in the presence of lipids. This has been proposed to account for channel formation through membranes [17], but not directly demonstrated. For the synthetic $(KL)_mK$ peptides, which are the first linear ones which both fold into ideally amphipathic β-sheets and display significant hemolytic activity, the β-sheets are necessarily formed by tigth intermolecular lock through hydrogen bonds, in principle able to grow up to very large structures. This cast some doubt on the concept that only the intramolecularly constrained β-sheets are sufficient to induce permeabilization of biological membranes [12,21,23].

Throughout this $(KL)_mK$ series, the hemolytic activity and the lipid affinity for mono- and bilayers linearly increased in parallel with peptide length

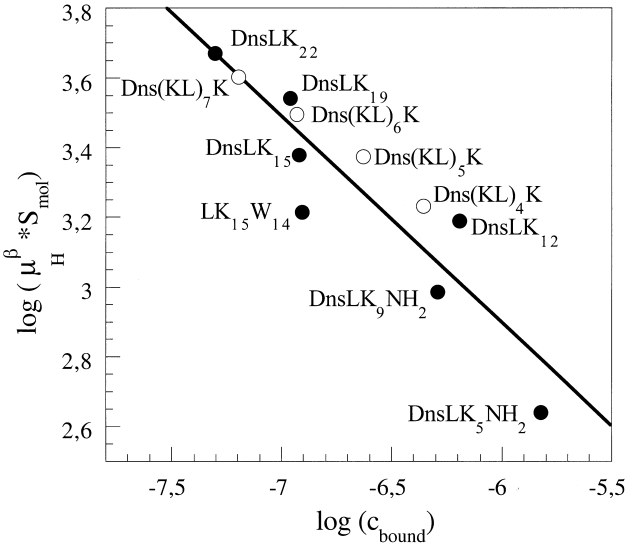

Fig. 10. Correlation between peptide physical properties determined in monolayer experiments and the peptide hemolytic efficiency defined as the bound peptide concentration, c_{bound}, required to induce 50% of hemolysis. μ_H^β is the calculated hydrophobic moment, S_{mol} is the peptide molecular area occupied at the interface. ○ $(KL)_mK$ (m=4–7), ● $(Dns)L_iK_j$ ($i=2j$) series [7,78], correlation factor $R=0.92$.

(Fig. 9). Each new added LK motif induces an increase in both lipid affinity and lytic activity. Therefore, the lipid affinity is a limiting factor for the lytic activity of these $(KL)_mK$ peptides. When compared to the LK peptides with a L/K = 2 ratio [6,78,79], the $(KL)_mK$ peptides display a lower lipid affinity and are less active. At the same total peptide length, the approximate 2.2 factor between their activities and affinities parallels the difference in L content throughout both series. Beyond the secondary ideally amphipathic character, hydrophobicity modulates both lipid affinity and lytic activity. This totally agrees with the conclusions from an α-helical LK series of 18 residues long peptides in which the L/K ratio varied from 0.3 to 2.6 [75].

The lytic efficiency can be defined as the bound peptide concentration, c_{bound}, required to induce the same perturbation on the erythrocyte membranes, for instance 50% hemolysis. The longer the peptide in this $(KL)_mK$ series, the lower the c_{bound} and, therefore, the more efficient the peptide is: one $(KL)_7K$ is as efficient as seven $(KL)_4K$. Therefore, other criteria which depend on the intrinsic properties of peptides also directly modulate lytic activity. For instance, there is a good correlation between hemolytic efficiency and the $\mu_H^\beta \times S_{mol}$ product, which takes into account the amphipathicity, the structure and the orientation at the interfaces (Fig. 10). Furthermore, there is no significant difference in the efficiency at similar length between the L/K = 2 and the L/K = 1 series (Fig. 10). Therefore, while hydrophobicity is a dominant factor for membrane affinity, it is not the only decisive one to induce lysis. As soon as they are bound, the ideally amphipathic β-sheets of the $(KL)_mK$ peptides are as efficient as the α-helices. Therefore, more than the nature of the secondary structure, it is the ideal amphipathic character which is decisive for efficiency.

To summarize, we report the first systematic study of a highly simplified synthetic series of linear $(KL)_mK$ peptides which fold into ideally amphipathic intermolecular antiparallel β-sheets when bound to zwitterionic lipids and are both hemolytic as shown herein and active on mycoplasma (L. Beven, S. Castano, K. Buttner, J. Dufourcq and H. Wroblewski, to be published). The first decisive step of lysis looks similar to the so-called 'raft' or 'carpet' models proposed for the α-helical peptides [7,78,80,81]: monomeric peptides invade the interface of the outer leaflet. However, they form probably large and rigid β-sheet structures lying flat at the interface with burying their poly-L face and increasing the outer leaflet area. Since there is no correlation between bilayer thickness and peptide length, it is the asymmetric disturbance in lipid organization that probably leads to a drastic and transient leakage of the inner content simultaneously to peptide interaction and accumulation.

Acknowledgements

We are pleased to acknowledge Dr Klaus Büttner at Fournier Pharma, Heidelberg, Germany, for providing the peptides used herein, Wilfrid Neri for their skilful purification, Alexandra Pinto da Silva for help in calcein assays and Dr Jean-Claude Talbot for fluorescence lifetime measurements. This work was supported in part by CNRS program GDR 790.

References

[1] I. Cornut, E. Thiaudière and J. Dufourcq, in: R.M. Epand (Ed.), The Amphipathic Helix. CRC Press, Boca Raton, FL, 1993, pp. 173–219.
[2] G. Saberwal, R. Nagaraj, Biochim. Acta 1197 (1994) 109–131.
[3] W.L. Maloy, U.P. Kari, Biopolymers 37 (1995) 105–122.
[4] P. Nicolas, A. Mor, Annu. Rev. Microbol. 49 (1995) 277–304.
[5] R.M. Kini, H.J. Evans, Int. J. Pept. Protein Res. 34 (1989) 277–286.
[6] S. Castano, I. Cornut, K. Büttner, J.L. Dasseux, J. Dufourcq, Biochim. Biophys. Acta 1416 (1999) 161–175.
[7] S. Castano, B. Desbat, M. Laguerre, J. Dufourcq, Biochim. Biophys. Acta 1416 (1999) 176–194.
[8] S.E. Blondelle, R.A. Houghten, Biochemistry 31 (1992) 12688–12694.
[9] M. Dathe, M. Schumann, T. Wieprecht, A. Winkler, M. Beyermann, E. Krause, K. Matsuzaki, O. Murase, M. Bienert, Biochemistry 35 (1996) 12612–12622.
[10] S. Lee, T. Iwata, H. Oyagi, H. Aoyagi, M. Ohno, K. Anzai, Y. Kirino, G. Sugihara, Biochim. Biophys. Acta 1151 (1993) 76–82.
[11] R.M. Epand, in: The Amphipathic Helix. CRC Press, Boca Raton, FL, 1993.
[12] S. Ando, H. Nishikawa, H. Takiguchi, S. Lee, G. Sugihara, Biochim. Biophys. Acta 1147 (1993) 42–49.

[13] K. Lohner, A. Latal, R.I. Lehrer, T. Ganz, Biochemistry 36 (1997) 1525–1531.
[14] P. Bougis, H. Rochat, G. Piéroni, R. Verger, Biochemistry 20 (1981) 4915–4920.
[15] P. Bougis, M. Tessier, J. Van Rietschoten, H. Rochat, J.F. Faucon, J. Dufourcq, Mol. Cell. Biochem. 55 (1983) 49–64.
[16] R.I. Lehrer, T. Ganz, M.E. Selsted, Cell 64 (1991) 229–230.
[17] C.P. Hill, J. Yee, M.E. Selsted, D. Eisenberg, Science 251 (1991) 1481–1485.
[18] R.E.W. Hancock, R. Lehrer, TIB TECH 16 (1998) 82–88.
[19] S. Conciancich, A. Ghazi, C. Hetru, J.A. Hoffman, L. Letellier, J. Biol. Chem. 268 (1993) 19239–19245.
[20] R. Maget-Dana, J.M. Bonmatin, C. Hetru, M. Ptak, J.C. Maurizot, Biochimie 77 (1995) 240–244.
[21] K. Matsuzaki, M. Nakayama, M. Fukui, A. Otaka, S. Funakoshi, N. Fuji, K. Bessho, K. Miyajima, Biochemistry 32 (1993) 11704–11710.
[22] A. Aumelas, M. Mangoni, C. Roumestand, L. Chiche, E. Despaux, G. Grassy, B. Calas, A. Chavanieu, Eur. J. Biochem. 237 (1996) 575–583.
[23] K. Matsuzaki, S. Yoneyama, N. Fujii, K. Miyajima, K. Yamada, Y. Kirino, K. Anzai, Biochemistry 36 (1997) 9799–9806.
[24] D. Romeo, B. Skerlavaj, M. Bolognesis, R. Gennaro, J. Biol. Chem. 263 (1988) 9573–9575.
[25] P.M. Hwang, N. Zhou, X. Shan, C.H. Arrowsmith, H.J. Vogel, Biochemistry 37 (1998) 4288–4298.
[26] M. Pezolet, L. Duchesneau, P. Bougis, J.F. Faucon, J. Dufourcq, Biochim. Biophys. Acta 704 (1982) 515–523.
[27] R. Maget-Dana, M. Ptak, Biophys. J. 73 (1997) 2527–2533.
[28] L.H. Kondejewski, S.W. Farmer, D.S. Wishart, C.M. Kay, R.E.W. Hancock, R.S. Hodges, J. Biol. Chem. 271 (1996) 25261–25268.
[29] A. Brack, G. Spach, J. Am. Chem. Soc. 103 (1981) 6319–6323.
[30] B. Barbier, M. Perello, A. Brack, Coll. Czech. Chem. Commun. 53 (1988) 2825–2832.
[31] S. Ono, S. Lee, H. Mihara, Y. Aoyagi, T. Kato, N. Yamasaki, Biochim. Biophys. Acta 1022 (1990) 237–244.
[32] S.E. Blondelle, B. Forood, R.A. Houghten, E. Perez-Paya, Biochemistry 36 (1997) 8393–8400.
[33] W.C. Wimley, K. Hristova, A.S. Ladhokin, L. Silvestro, P.H. Axelsen, S.H. White, J. Mol. Biol. 277 (1998) 1091–1110.
[34] D. Osterman, R. Mora, F.J. Kezdy, E.T. Kaiser, S.C. Meredith, J. Am. Chem. Soc. 106 (1984) 6845–6847.
[35] E. Krause, M. Beyermann, H. Fabian, M. Dathe, S. Rothemund, M. Bienert, Int. J. Pept. Protein Res. 48 (1996) 559–568.
[36] W.F. De Grado, J.D. Lear, J. Am. Chem. Soc. 107 (1985) 7684–7689.
[37] S.E. Blondelle, J. Ostrech, R.A. Houghten, E. Pérez-Paya, Biophys. J. 68 (1995) 351–359.
[38] S. Castano, B. Desbat, I. Cornut, P. Méléard, J. Dufourcq, Lett. Pept. Sci. 4 (1997) 195–200.
[39] D. Blaudez, T. Buffeteau, J.C. Cornut, B. Desbat, N. Escafre, M. Pezolet, J.M. Turlet, Thin Solid Films 242 (1994) 146–150.
[40] D. Blaudez, J.M. Turlet, J. Dufourcq, D. Bard, T. Buffeteau, B. Desbat, J. Chem. Soc. Faraday Trans. 92 (1996) 525–530.
[41] I. Cornut, B. Desbat, J.M. Turlet, J. Dufourcq, Biophys. J. 70 (1996) 305–312.
[42] M. Boncheva, H. Vogel, Biophys. J. 73 (1997) 1056–1072.
[43] I. Cornut, K. Büttner, J.L. Dasseux, J. Dufourcq, FEBS Lett. 349 (1994) 29–33.
[44] E. Perez-Paya, J. Dufourcq, L. Braco, C. Abad, Biochim. Biophys. Acta 1323 (1997) 223–236.
[45] J. Dufourcq, J.F. Faucon, G. Fourche, J.L. Dasseux, M. Le Maire, T. Gulik-Krzywicki, Biochim. Biophys. Acta 859 (1986) 33–48.
[46] N. Oku, D.A. Kendall, R.C. Mac Donald, Biochim. Biophys. Acta 691 (1982) 3332–3340.
[47] F. Perrin, Ann. Phys. 12 (1929) 213–275.
[48] T.L. Mac Meekin, M.L. Groves, N.J. Hipp, J. Am. Chem. Soc. 71 (1949) 3298–3300.
[49] C. Tanford, in: Physical Chemistry of Macromolecules. Wiley, New York, 1967, pp. 339–342.
[50] J. Yguerabide, Methods Enzymol. 26 (1972) 498–578.
[51] L.K. Tamm, in: S. White (Ed.), Membrane Protein Structure. Oxford University Press, 1994, pp. 283–313.
[52] A.F. Mingotaud, C. Mingotaud and L.K. Patterson, in: Handbook of Monolayers, Vol. 2, Harcourt Brace Jovanovitch, San Diego, p. 782.
[53] D. Eisenberg, R.M. Weiss, T.C. Terwilliger, Nature 299 (1982) 371–374.
[54] S.E. Blondelle, R.A. Houghten, Biochemistry 30 (1991) 4671–4678.
[55] T. Miyazawa, in: Infrared Spectra and Helical Conformations. M. Dekker, NY, 1967.
[56] W.K. Surewicz, H.H. Mantsch, D. Chapman, Biochemistry 32 (1993) 389–394.
[57] E. Goormaghtigh, V. Cabiaux and J.M. Ruysschaert, in: H.J. Hilderson and G.B. Ralston (Eds.), Subcellular Biochemistry: Physicochemical Methods in the Study of Biomembranes, Vol. 23, Plenum Press, New York, 1994, pp. 405–450.
[58] S. Krimm, J. Bandekar, Adv. Protein Chem. 38 (1986) 181–364.
[59] P.I. Haris, D. Chapman, TIBS 17 (1992) 328–333.
[60] S.A. Tatulian, L.R. Jones, L.G. Reddy, D.L. Stokes, L.K. Tam, Biochemistry 34 (1995) 4448–4456.
[61] T. Buffeteau, B. Desbat, Appl. Spectrosc. 43 (1989) 1027–1032.
[62] J.E. Bertie, Z. Lan, Appl. Spectrosc. 50 (1996) 1047–1057.
[63] D. Marsh, Biophys. J. 72 (1997) 2710–2718.
[64] R.E. Dickerson and I. Geis, in: The Structure and Action of Proteins. Harper Row, New York, 1969.
[65] J.A. Reynaud, J.P. Grivet, D. Sy, Y. Trudelle, Biochemistry 32 (1993) 4997–5008.
[66] S.H. White, W.C. Winley, Curr. Opin. Struct. Biol. 4 (1994) 79–86.

[67] T.E. Creighton, in: Proteins, Structure and Molecular Properties. W.H. Freeman and Company, New York, 1996.
[68] S.H. Portlock, Y. Lee, J. Tomich, L.K. Tamm, J. Biol. Chem. 267 (1992) 11017–11022.
[69] G. Schwarz, G. Beschiaschvili, Biochim. Biophys. Acta 979 (1989) 82–90.
[70] Z. Oren, J. Hong, Y. Shai, Eur. J. Biochem. 259 (1999) 360–369.
[71] A.J. Verkleij, R.F. Zwaal, B. Roelofsen, P. Confurius, D. Kasteljin, L.L.M. Van Deenen, Biochim. Biophys. Acta 323 (1973) 178–193.
[72] C. Branden and J. Tooze, in: Introduction to Protein Structure. Garland Publ., New York, 1991.
[73] M. Weiss, G.E. Schulz, J. Mol. Biol. 227 (1992) 493–509.
[74] B. Bechinger, J. Mol. Biol. 263 (1996) 768–775.
[75] T. Kiyota, S. Lee, G.V. Sugihara, Biochemistry 35 (1996) 13196–13204.
[76] S.H. White, W.C. Wimley, A.S. Ladokhin and K. Hristova, Methods of Enzymology part B 295 (1998) 62–87.
[77] B.H. Bull, K. Breese, Arch. Biochem. Biophys. 161 (1974) 665–670.
[78] S. Castano, I. Cornut, P. Méléard, K. Büttner, B. Desbat and J. Dufourcq, in: R. Ramage and R. Epton (Eds.), Peptides 1996. Escom, 1997, pp. 297–298.
[79] I. Cornut, K. Bütner, L. Beven, H. Duclohier and J. Dufourcq, in: H.L.S. Maïa (Ed.), Peptides 1994. Escom, Leide, 1995, pp. 666–667.
[80] G. Raghunathan, P. Seetharamulu, B.R. Brooks, H.R. Guy, Proteins 8 (1990) 213–225.
[81] Y. Shai, Z. Oren, J. Biol. Cell. 271 (1996) 7305–7308.